J. Fluid Mech. (1999), *vol.* 385, *pp.* 41–62. Printed in the United Kingdom

Lattice-Boltzmann simulations of particles in non-zero-Reynolds-number flows

By DEWEI QI

Department of Paper and Printing Science and Engineering, Western Michigan University, Kalamazoo, MI 49008, USA

(Received 14 November 1997 and in revised form 13 October 1998)

A lattice-Boltzmann method has been developed to simulate suspensions of both spherical and non-spherical particles in finite-Reynolds-number flows. The results for sedimentation of a single elliptical particle are shown to be in excellent agreement with the results of Huang, Hu & Joseph (1998) who used a finite-element method. Sedimentation of two-dimensional circular and rectangular particles in a two-dimensional channel and three-dimensional spherical particles in a tube with square cross-section is simulated. Computational results are consistent with experimentally observed phenomena, such as drafting, kissing and tumbling.

1. Introduction

Spherical and non-spherical particles in flows at finite Reynolds number occur in a variety of industries, such as the petroleum and paper industries. This subject has been studied theoretically and experimentally for many years. Numerical simulations have been extensively used to simulate complex particle–fluid systems. Stokesian simulations were developed by Brady & Bossis (1988) to deal with the motion of many particles in Stokes flow. These simulations are appropriate for colloidal particles at very small Reynolds numbers. Chang & Powell (1993) conducted Stokesian simulations for a bimodal suspension of spherical particles. However, for finite-Reynolds-number flows, the inertial term has a significant influence on the behaviour of solid particles and fluid. In such systems, the Navier–Stokes equations should be solved to produce valid results. Johnson & Tezduyar (1997) conducted a three-dimensional simulation using a space–time finite-element method advocated by Hughes, Franca & Mallet (1987) and Tezduyar *et al.* (1992). The sedimentation of 100 solid spheres in a tube at a Reynolds number of 100 was simulated. Joseph's group (Hu, Joseph & Crochet 1992; Feng, Hu & Joseph 1994*a*, *b*) developed a direct simulation of the two-dimensional motion of circular and elliptical particles in sedimenting, Couette, and Poiseuille flows of a Newtonian fluid at particle Reynolds numbers in the hundreds. Recently, Hu (1996) simulated the motion of 400 circular particles in sedimenting and shear flows at particle Reynolds numbers up to hundreds.

All the simulations mentioned above are based on the finite-element or finite-difference method. An approach, called lattice-Boltzmann (LB) simulation, has been developed to simulate suspensions including three-dimensional spherical, non-spherical particles (Ladd 1994*a*, *b*; Aidun & Lu 1995; Qi 1997*a*, *b*) and deformable membranes (Aidun & Qi 1998). This work develops the LB method to simulate spherical and non-spherical particles in finite-Reynolds-number flows. The validity of this approach is demonstrated.

A brief review of the LB method is given in § 2.1. An improvement to the Ladd approach is described in § 2.2. A summary of calculations for three-dimensional rotation is given in § 2.3. The results of the LB method for the sedimentation of a single elliptical particle at particle Reynolds numbers $Re = 0.31$, 0.82 and 16.8 are compared with the finite element results in § 3.1. Sedimentation of two-dimensional circular particles is simulated in § 3.2, and of two rectangular particles in § 3.3. Sedimentation of two three-dimensional spheres is modelled in a tube in § 3.4. Conclusions are drawn in the final section.

2. Theoretical method

Lattice-gas automata and the three-dimensional lattice-Boltzmann method (Wolfram 1986; d'Humieres, Lallemand & Frisch 1986; d'Humieres & Lallemand 1987; Frisch *et al.* 1987; McNamara & Zanetti 1988; Qian, d'Humieres & Lallemand 1992; Dahlburg, Montgomery & Doolen 1987) have been developed to simulate the interaction between fluid and solid particles. These methods have become useful tools to solve the Navier–Stokes equations in suspensions and in complex random porous media (Gunstensen & Rothman 1991*a*, *b*). The LB method simulates fluid motion at a microscopic level, similar to a molecular dynamic simulation. It has been proven that the Navier–Stokes equations are fully recovered at the macroscopic scale through a Chapman–Enskog-like expansion (Chen, Chen & Matthaeus 1992).

A lattice-gas method was developed to simulate 100 colloidal particles by Ladd, Colvin & Frenkel (1988) and Ladd & Frenkel (1990). A collision rule in the lattice-gas method was proposed to deal with the moving boundaries. Later, Ladd (1994*a*) extended the LB method to model spherical particles. He simulated two-dimensional circular and 32 000 three-dimensional spherical particles (Ladd 1996, 1997) using the extension. Suspensions of spherical particles and their rheological properties at a high concentration were simulated by Aidun & Lu (1995). Three-dimensional rotation and translations of non-spherical particles including ellipsoid, cylinders, and cubic-shaped particles were modelled with the LB method by Qi (1997*a–c*) and Aidun, Lu & Ding (1998). A brief review of the method follows.

2.1. *Lattice-Boltzmann method*

In the LB method, the fluid particles reside at nodes in a lattice and move to neighbouring nodes. The fluid particle movement represents real fluid flows through a distribution function of fluid particle density. There are two speeds of moving fluid particles in addition to fluid particles at rest. The particles of speed $\sigma = 1$ move along links of the lattice in axial directions and the particles of speed $\sigma = 2$ move along the diagonal links of the lattice. The solid particles are discretized and move across the stationary lattice. The hydrodynamic forces and torques acting on the solid particle can be determined from a summation of the momentum of all the fluid particles hitting the solid particle boundaries. Then the motion of the solid particles is determined at each time step from the forces and the torques by using Newton's second law, called molecular dynamics simulations in computer simulation terminology. In principle, this simulation method is very flexible. Solid particle size and shape, electrostatic interactions, flow geometry, Péclet number, and Reynolds number can all be varied independently.

In this work, a 9-bit model is employed for two-dimensional case and a 15-bit model for three-dimensional (Qian 1990) case. Although, the simulations do not involve bit-wise operations, the terms '9-bit' and '15-bit' are maintained for historical

σ	i	$e_{\sigma ix}$	$e_{\sigma iy}$	$\lvert e_{\sigma i}\rvert$	σ	i	$e_{\sigma ix}$	$e_{\sigma iy}$	$\lvert e_{\sigma i}\rvert$
1	1	1	0	1	2	1	1	1	$\sqrt{2}$
1	2	−1	0	1	2	2	−1	−1	$\sqrt{2}$
1	3	0	1	1	2	3	−1	1	$\sqrt{2}$
1	4	0	−1	1	2	4	1	−1	$\sqrt{2}$

TABLE 1. Velocity vector for cubic lattice in two dimensions.

σ	i	$e_{\sigma ix}$	$e_{\sigma iy}$	$e_{\sigma iz}$	$\lvert e_{\sigma i}\rvert$	σ	i	$e_{\sigma ix}$	$e_{\sigma iy}$	$e_{\sigma iz}$	$\lvert e_{\sigma i}\rvert$
1	1	1	0	0	1	2	1	1	1	1	$\sqrt{3}$
1	2	−1	0	0	1	2	2	−1	−1	−1	$\sqrt{3}$
1	3	0	1	0	1	2	3	−1	1	1	$\sqrt{3}$
1	4	0	−1	0	1	2	4	1	−1	−1	$\sqrt{3}$
1	5	0	0	1	1	2	5	−1	−1	1	$\sqrt{3}$
1	6	0	0	−1	1	2	6	1	1	−1	$\sqrt{3}$
						2	7	1	−1	1	$\sqrt{3}$
						2	8	−1	1	−1	$\sqrt{3}$

TABLE 2. Velocity vector for cubic lattice in three dimensions.

reasons. Complete lists of the velocities of fluid particles, $\boldsymbol{e}_{\sigma i}$, are given in table 1 for the two-dimensional case and in table 2 for three-dimensional case.

The lattice-Boltzmann (LB) equation with a single relaxation time (Chen *et al.* 1992) is

$$f_{\sigma i}(\boldsymbol{x}+\boldsymbol{e}_{\sigma i}, t+1) - f_{\sigma i}(\boldsymbol{x}, t) = -\frac{1}{\tau}[f_{\sigma i}(\boldsymbol{x}, t) - f^{(0)}_{\sigma i}(\boldsymbol{x}, t)], \tag{2.1}$$

where $f_{\sigma i}(\boldsymbol{x}, t)$ is the fluid particle distribution function, $f^{(0)}_{\sigma i}(\boldsymbol{x}, t)$ is the equilibrium distribution function (EDF) at $(\boldsymbol{x}, t)$ and τ is the single relaxation time. The kinematic viscosity v is related to τ by $v = (2\tau - 1)/6$. In the simulations, $f^{(0)}_{\sigma i}(\boldsymbol{x}, t)$ is taken as

$$f^{(0)}_{\sigma i}(\boldsymbol{x}, t) = A_\sigma + B_\sigma(\boldsymbol{e}_{\sigma i}\cdot\boldsymbol{u}) + C_\sigma(\boldsymbol{e}_{\sigma i}\cdot\boldsymbol{u})^2 + D_\sigma u^2, \tag{2.2}$$

where $\sigma = 1$ corresponds to the fluid particles moving to the near-neighbours along axial directions; $\sigma = 2$ corresponds to the fluid particles moving to their second-near neighbours along diagonal directions; $\sigma = 0$ and $i = 0$ correspond to the fluid particles at rest; $\boldsymbol{e}_{\sigma i}$ is the vector of both lattice spacing and fluid particle velocity; $\boldsymbol{u}$ is the mean velocity of fluid particles. Following the Ladd method (Ladd 1994*a*), appropriate coefficients are found for the two-dimensional case:

$$\left.\begin{aligned} A_1 = \tfrac{1}{9}\rho_f, \quad B_1 = \tfrac{1}{3}\rho_f \quad C_1 = \tfrac{1}{2}\rho_f, \quad D_1 = -\tfrac{1}{6}\rho_f, \\ A_2 = \tfrac{1}{36}\rho_f, \quad B_2 = \tfrac{1}{12}\rho_f \quad C_2 = \tfrac{1}{8}\rho_f, \quad D_2 = -\tfrac{1}{24}\rho_f, \\ A_0 = \tfrac{4}{9}\rho_f, \quad D_0 = -\tfrac{2}{3}\rho_f; \end{aligned}\right\} \tag{2.3}$$

and for the three-dimensional (Qian 1990) case:

$$\left.\begin{aligned} A_1 = \tfrac{1}{9}\rho_f, \quad B_1 = \tfrac{1}{3}\rho_f \quad C_1 = \tfrac{1}{2}\rho_f, \\ D_1 = -\tfrac{1}{6}\rho_f, \quad A_2 = \tfrac{1}{72}\rho_f, \quad B_2 = \tfrac{1}{24}\rho_f, \\ C_2 = \tfrac{1}{16}\rho_f, \quad D_2 = -\tfrac{1}{48}\rho_f, \quad A_0 = \tfrac{2}{9}\rho_f, \\ D_0 = -\tfrac{1}{6}\rho_f, \end{aligned}\right\} \tag{2.4}$$

where ρ_f is the density of the fluid.

2.2. *Hydrodynamic forces on a solid particle*

Ladd's (1994*a*) approach can be divided into two parts: the first accounts for the moving boundary conditions and the second part is to calculate the hydrodynamic forces exerted on solid particles.

Regarding the first part, if the solid is stationary, a no-slip boundary condition is easily implemented by using the bounce-back method. However, the bounce-back method is not suitable for moving boundaries and must be modified. Ladd proposed a collision rule which is given by

$$f_{\sigma i'}(\boldsymbol{x}, t+1) = f_{\sigma i}(\boldsymbol{x}, t_+) - 2B_\sigma(\boldsymbol{e}_{\sigma i} \cdot \boldsymbol{V}_b), \tag{2.5}$$

where $\boldsymbol{x}$ is the position of the node adjacent to the solid surface with velocity $\boldsymbol{V}_b$, t_+ is the post-collision time, as defined in Ladd (1994*a*), i' denotes the reflected direction, and i the incident direction. The above rule is applied to the boundary nodes on both sides of the solid surface. As a result, the velocity of the solid boundary matches the velocity of the fluid. In other words, a no-slip boundary condition for moving solid particles is imposed correctly by Ladd's collision rule in such a way that the fluid mass is conserved at each time step by allowing exchange of population of fluid at the boundary nodes adjacent to both sides of the solid surface.

The hydrodynamic force exerted on the solid particle at the boundary node is

$$F(\boldsymbol{x} + \tfrac{1}{2}\boldsymbol{e}_{\sigma i}) = 2\boldsymbol{e}_{\sigma i}(f_{\sigma i}(\boldsymbol{x}, t_+) - B_\sigma(\boldsymbol{V}_b \cdot \boldsymbol{e}_{\sigma i})), \tag{2.6}$$

where $\boldsymbol{V}_b = \boldsymbol{V} + \Omega \times \boldsymbol{x}_b$; $\boldsymbol{V}$ is the velocity of the centre of mass of a solid particle; $\boldsymbol{V}_b$ is the velocity of the solid–fluid interface at the node; Ω is the angular velocity of the solid particle; $\boldsymbol{x}_b = \boldsymbol{x} + \frac{1}{2}\boldsymbol{e}_{\sigma i} - \boldsymbol{R}$, where $\boldsymbol{R}$ is the centre of mass of the corresponding solid particle. The total force F_T and torque T_T on the solid particles are

$$F_T = \sum F(\boldsymbol{x} + \tfrac{1}{2}\boldsymbol{e}_{\sigma i}) \tag{2.7}$$

and

$$T_T = \sum (\boldsymbol{x} + \tfrac{1}{2}\boldsymbol{e}_{\sigma i} - \boldsymbol{R}) \times F(\boldsymbol{x} + \tfrac{1}{2}\boldsymbol{e}_{\sigma i}). \tag{2.8}$$

The summation is over all the boundary nodes in both the solid and fluid regions. When the effective density, $\rho_e = \rho_s - \rho_f$, of the solid particle is used for updating the motion of the solid particles in Newtonian dynamics (Ladd 1994*a*), where ρ_s is the solid density, the results from Ladd's approach are in excellent agreement with the finite-element results. A comparison will be made in the results section. The advantage of this method is that the computational implementation is simple, and dynamical simulations are very stable. A small simulation box may be used to reach a high Reynolds number. However, a disadvantage is that this method cannot handle a solid density less than that of the fluid.

Therefore, seeking an improvement to the Ladd approach is necessary. Aidun *et al.* (1998) attempted to improve Ladd's approach by removing the fluid within the solid region.

In the lattice-Boltzmann method, the nodes are fixed and the solid particles move across the nodes (grids). A boundary node in the fluid region at a previous time step may enter the solid region at the next time step. Therefore, the flow at the node should exert a force F_I on the solid particle

$$F_I(\boldsymbol{x}, t) = \rho_f(\boldsymbol{x}, t)\boldsymbol{u}(\boldsymbol{x}, t), \tag{2.9}$$

where ρ_f is the density of the fluid at the node. Similarly, a boundary node originally within the solid region may be within the fluid region at the next time step. The flow at the node should exert a force F_O on the solid particle, i.e.

$$F_O(\boldsymbol{x}, t) = -\rho_f(\boldsymbol{x}, t)\boldsymbol{u}(\boldsymbol{x}, t). \tag{2.10}$$

The forces and torques should be added to the total force and torques, while the force and torque from equations (2.7) and (2.8) at interior nodes of a solid should not add to the total force in the present method. The equations (2.9) and (2.10) are essentially the same as those suggested in Aidun *et al.* (1998).

There are good reasons to allow fluid to enter the solid region as Ladd did. First, the total mass of fluid in the simulation box is strictly conserved at each time step. This restriction guarantees recovery of the Navier–Stokes equations from the LB method. Second, in the present method, the function of the fluid within the solid region is to ensure that the Navier–Stokes equations are followed in the fluid region.

2.3. *Three-dimensional rotation and translation of non-spherical particles*

A proper calculation for the rotation of non-spherical particles in a three-dimensional space is important in simulations. The problem has been discussed by Qi (1997*a*, *b*).

The orientation of a rigid solid body specifies the relation between a laboratory coordinate system and a body coordinate system which is fixed on the rigid solid body. The Euler angles ϕ, θ and ψ are used to describe the three-dimensional rotation of the body (Goldstein 1980). The body coordinate system is rotated around the z-axis by ϕ, then rotated around the x'-axis by θ and rotated again around the new z'-axis by ψ. The inertia tensor of the particle is diagonal in the body coordinate system.

The motion of rotation is governed by the Euler equations, which are written

$$\dot{\Omega}_x = \frac{\tau_x}{I_{xx}} + \frac{I_{yy} - I_{zz}}{I_{xx}}\Omega_y\Omega_z, \tag{2.11}$$

$$\dot{\Omega}_y = \frac{\tau_y}{I_{yy}} + \frac{I_{zz} - I_{xx}}{I_{yy}}\Omega_z\Omega_x, \tag{2.12}$$

$$\dot{\Omega}_z = \frac{\tau_z}{I_{zz}} + \frac{I_{xx} - I_{yy}}{I_{zz}}\Omega_x\Omega_y, \tag{2.13}$$

where Ω_x, Ω_y and Ω_z are the angular velocities in the body coordinate system, and τ_x, τ_y and τ_z are the torques exerted on the solid particle in the same coordinate system. I_{xx}, I_{yy} and I_{zz} are the inertia of the solid particles. Unfortunately, use of the Euler angles results in a singularity in the equations of motion whenever θ approaches 0 or π. Therefore, Euler angles are not appropriate for solving the equation directly, instead four quaternion parameters must be used as generalized coordinates (Evans 1977; Evans & Murad 1997) to avoid the singularity. The relationships between the quaternion parameters and the Euler angles are defined by

$$q_0 = \cos\tfrac{1}{2}\theta\cos\tfrac{1}{2}(\phi+\psi), \tag{2.14}$$

$$q_1 = \sin\tfrac{1}{2}\theta\cos\tfrac{1}{2}(\phi-\psi), \tag{2.15}$$

$$q_2 = \sin\tfrac{1}{2}\theta\sin\tfrac{1}{2}(\phi-\psi), \tag{2.16}$$

and

$$q_3 = \cos\tfrac{1}{2}\theta\sin\tfrac{1}{2}(\phi+\psi). \tag{2.17}$$

The transformation matrix from the coordinate system to the body coordinate system is given by

$$\begin{pmatrix} q_0^2+q_1^2-q_2^2-q_3^2 & 2(q_1q_2+q_0q_3) & 2(q_1q_3-q_0q_2) \\ 2(q_1q_2-q_0q_3) & q_0^2-q_1^2+q_2^2-q_3^2 & 2(q_2q_3+q_0q_1) \\ 2(q_1q_3+q_0q_2) & 2(q_2q_3-q_0q_1) & q_0^2-q_1^2-q_2^2+q_3^2 \end{pmatrix}. \tag{2.18}$$

The quaternion for each solid particle satisfies the equations of motion

$$\begin{pmatrix} \dot{q}_0 \\ \dot{q}_1 \\ \dot{q}_2 \\ \dot{q}_3 \end{pmatrix} = \begin{pmatrix} q_0 & -q_1 & -q_2 & -q_3 \\ q_1 & q_0 & -q_3 & q_2 \\ q_2 & q_3 & q_0 & -q_1 \\ q_3 & -q_2 & q_1 & q_0 \end{pmatrix} \begin{pmatrix} 0 \\ \Omega_x \\ \Omega_y \\ \Omega_z \end{pmatrix}. \tag{2.19}$$

Equations (2.11), (2.12), (2.13) and (2.19) are solved by using the Gear predictor-corrector method (Gear 1971).

The translations of the centre of mass of each particle are updated at each Newtonian dynamic time step by using a so-called half-step 'leap-frog' scheme which is popular in molecular dynamic simulations (Allen & Tildesley 1987). The scheme is written as

$$\boldsymbol{V}(t+\tfrac{1}{2}\delta t) = \boldsymbol{V}(t-\tfrac{1}{2}\delta t) + \delta t\boldsymbol{F}(t)/M, \tag{2.20}$$

$$\boldsymbol{R}(t+\delta t) = \boldsymbol{R}(t) + \delta t\boldsymbol{V}(t-\tfrac{1}{2}\delta t) + \delta t^2\boldsymbol{F}(t)/M + O(\delta t^4), \tag{2.21}$$

where $\boldsymbol{R}$ is the position of the centre of mass of a solid particle, $\boldsymbol{F}$ is the total force on the solid particle, M is the mass of the solid particle.

Both the position and velocity of solid particles in equations (2.20) and (2.21) are expanded in the time interval δt explicitly. Therefore the time step δt for solid particles should be less than 1 to ensure accuracy within the fourth order of δt (Allen & Tildesley 1987). This is a standard technique in molecular dynamics simulations. The same applies to the calculation of the three-dimensional rotation of solid particles.

In the following sections, the present approach is applied to several simulation problems.

3. Simulations and results

3.1. *Sedimentation of a single two-dimensional ellipse*

For comparison, a single ellipse sedimenting under gravity is simulated under the same conditions as used by Huang, Hu & Joseph (1988), who solved the problem using a finite-element method. The elliptic particle rests initially at the middle of a two-dimensional channel and the major axis of the ellipse tilts at 135° with the horizontal direction. The width of the channel is 5 times of the length of the major axis D. The ratio of the length of the major axis to the short axis of the ellipse is 1.5 and the size of the simulation box is 101×700. The elliptic particle is heavier than

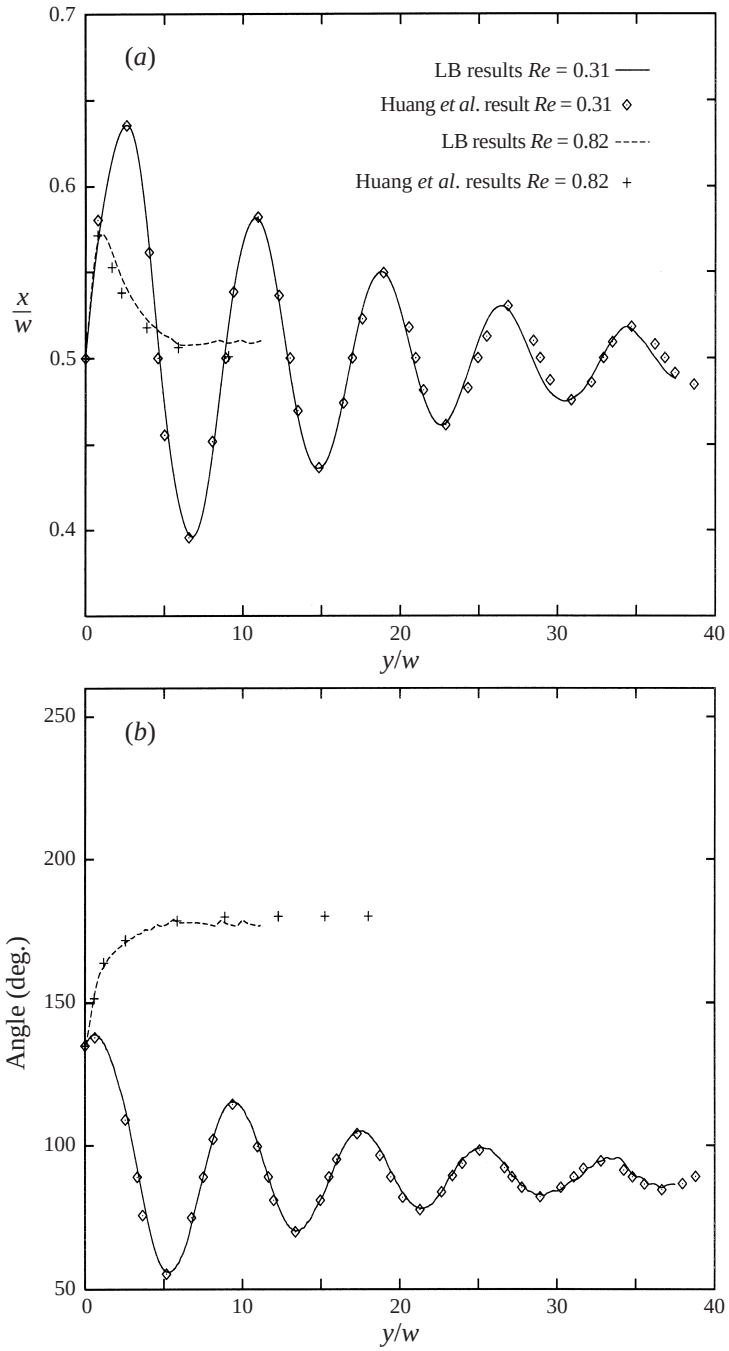

FIGURE 1. Comparison of the LB results with Huang *et al.* (1988) results for an ellipse sedimenting in a two-dimensional channel. (*a*) Displacement x as a function of y is shown; x is the horizontal direction and y is the gravity direction or vertical direction. (*b*) Rotational angles as a function of y are shown. Note that at $Re = 0.32$ the ellipse axis approaches 90° or horizontal, while at $Re = 0.31$ the ellipse adopts a 180° or vertical orientation. LB results are in excellent agreement with the results of Huang, Hu & Joseph (1998).

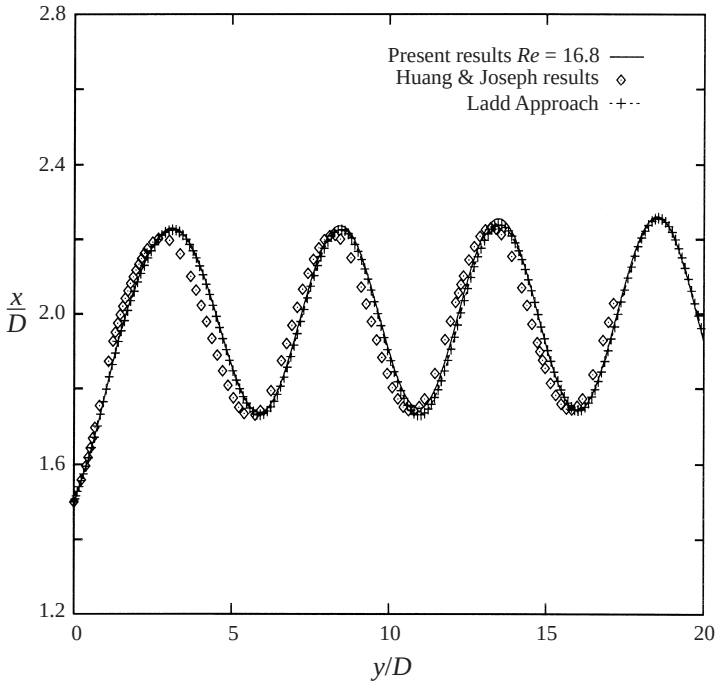

FIGURE 2. Comparison of the LB results for the displacement of an ellipse with Huang & Joseph's unpublished results at $Re = 16.8$. The dashed lines are the results from the Ladd approach.

the fluid and settles by gravity. The ratio of solid density to fluid density is 1.0015 for final particle Reynolds number $Re = 0.31$, and 1.005 for $Re = 0.82$. The final particle Reynolds number is defined by $Re = V_f D/2v$, where V_f is the final velocity of the particle. The inflow boundary is always placed $15D$ ahead of the elliptic particle and the flow velocity at the boundary is zero. The outflow boundary is always $20D$ behind the particle and the derivatives of flow velocity in x- and y-directions at the boundary are equal to zero.

The LB results are compared with the finite-element results obtained recently by Huang *et al.* (1998). Excellent agreement between two methods is clearly seen from figure 1. In all the figures of this work, displacement has been normalized by D, time normalized by D/V_f, velocity by V_f, and angular velocity by V_f/D, unless otherwise specified. Figure 1 shows that the lubrication pressure turns the ellipse vertical and it executes a damped oscillation as it drifts to the channel centre for the case of $Re = 0.31$, while the force couples on the long axis turn the ellipse horizontal for the case of $Re = 0.82$ as it migrates to the channel centre. The final position of the ellipse is slightly shifted from the channel centre with an error of 2.3% in the simulation box of 101×700 and with an error of 2.0% in a simulation box of 151×1050. This error is caused by discretization of the solid particle.

It has been pointed out by D. D. Joseph that it was originally thought that the ellipse would turn horizontal at any Reynolds number greater than zero. However, Joseph's new findings are confirmed by his experiment and simulation and are reproduced here.

To further evaluate the reliability of the LB method, a simulation of the sedimen-

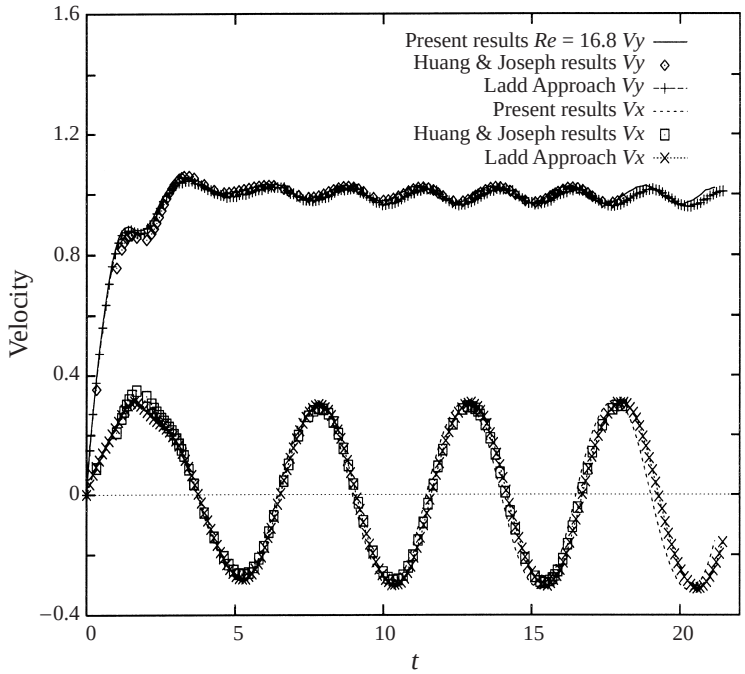

FIGURE 3. Comparison of the velocity in the x- and y- direction of LB results with Huang & Joseph's unplublished results for an ellipse sedimenting in a two-dimensional channel at $Re = 16.8$. The negative value of the velocity of particle settling under gravity is V_y. The same applies to the other figures.

tation of an ellipse is carried out for the case of $Re = 16.8$ using present approach. The ratio of the major axis length ($D = 28$) to the short axis of the ellipse is 2 and the ratio of the solid density to the fluid density is 1.5. The simulation box size is 113×1260. The ellipse is placed at $x = 0.375W$, where the width of the channel $W = 4D$. The tilting angle of the major axis with the horizontal direction (x-axis) is 135°. The inflow boundary is always $25D$ ahead of the particles and the derivative of the flow velocity at the boundary is zero. The outflow boundary is always $20D$ behind the particle and the flow velocity at the boundary is zero, i.e. the inflow and outflow boundaries move with the solid particle during the simulation. The results for the simulations are shown in figure 2 to figure 4 and compared with unpublished 1997 results of P. Y. Huang & D. D. Joseph (available from the author). Figure 2 shows the displacement of the ellipse: the dash-line is the result obtained by using the Ladd approach; the solid line is the present result; and the diamonds are the results of Huang & Joseph. It is obvious that both the present results and those obtained using the Ladd approach agree with the finite-element results. Figure 3 shows the velocities of the ellipse in the x- and y-directions, and figure 4 shows the rotation angle and angular velocity. All quantities including velocities and tilting angles in these figures are in excellent agreement with the finite-element results. At $Re = 16.8$, the position of the ellipse oscillates periodically around the centre of the channel, and the tilting angle oscillates around 180°. This is consistent with the experimental observation that the long axis of an ellipse is perpendicular to streamlines of the flows. The same simulations are repeated in a large simulation box of 168×1890. Essentially the same results are obtained.

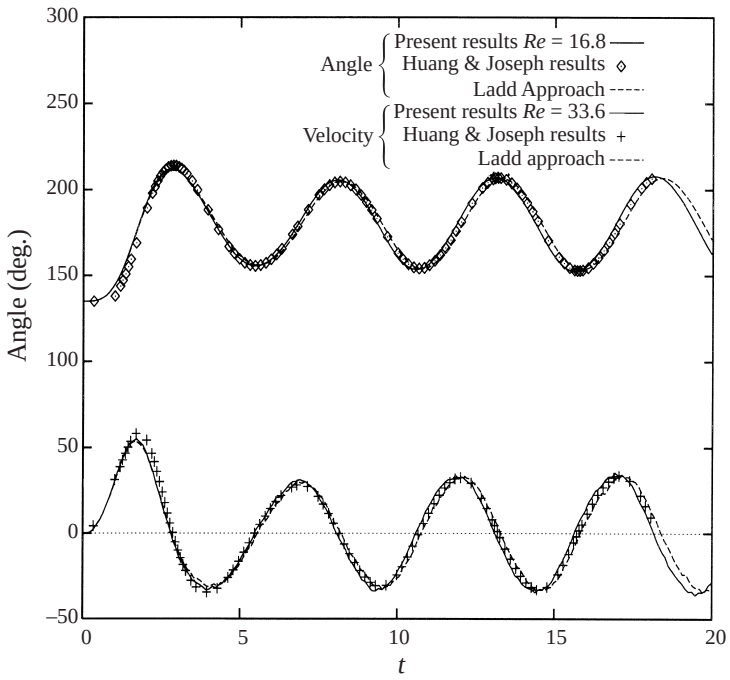

FIGURE 4. Comparison of the rotational angles and the angular velocities of the LB results with Huang & Joseph's unpublished results for an ellipse sedimenting in a two-dimensional channel at $Re = 16.8$.

3.2. *Sedimentation of two circular particles in two-dimensions*

An important feature of suspensions in finite Reynolds number flows is the so-called drafting, kissing, and tumbling (DKT) which was first experimentally discovered by Joseph *et al.* (1987) and then confirmed by computer simulations (Feng *et al.* 1994*a*, *b*). When solid particles sediment under gravity, the trailing particle will approach the leading particle due to the low pressure in the wake of the leading particle. This is the drafting stage. Then the trailing particle is accelerated and rapidly sucked into the wake, and the particle contacts the leading particle. This is called kissing. The alignment of two particles in the stream direction is not stable. A slight misalignment will push the front particle aside; the particle behind takes the lead; and then they are separated (dispersed). This is called tumbling. DKT may repeat many times and is a feature of Navier–Stokes flows in which inertia is important. Stokes flow does not have this feature. The scenario of DKT is used to test simulations of the finite Reynolds number suspension. The simulation of sedimentation of two circular particles is conducted in a box with a size of 121×405. The diameter of the particles D is 15. The two circular particles are put $2D$ apart along the gravity direction and aligned at $x = 0.25W$. The outflow boundary is kept at $15D$ behind the particle and the inflow boundary is $10D$ ahead of the particle during the simulation. The flow velocities at the boundaries are the same as before. The initial outflow boundary is at $y = 405$ and gravity is in the negative y-direction, while the initial inflow boundary is at $y = 0$. The ratio of solid density to fluid density is 2 and the particle Reynolds number is 5.6. The trailing particle becomes the leading one at $t = 11$ and $t = 58$ as shown in figure 5. The two particles exchange positions

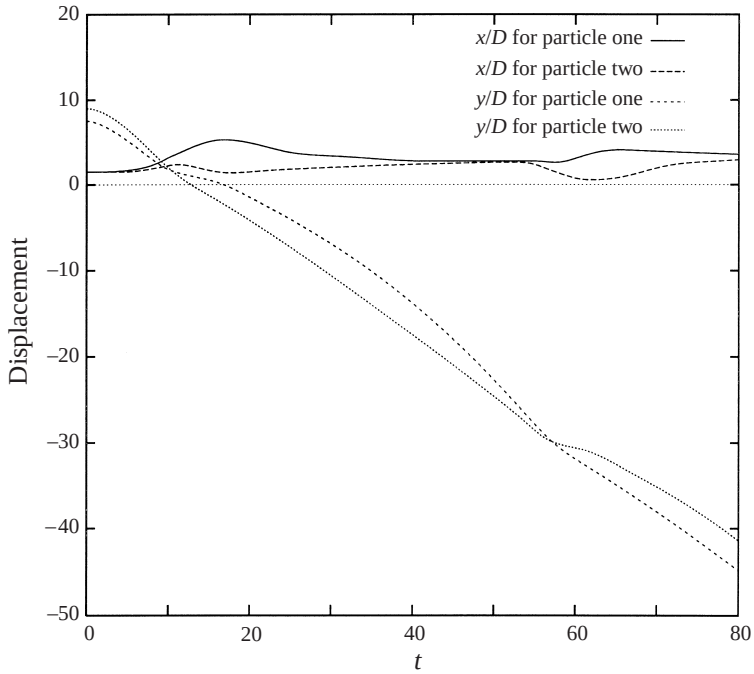

FIGURE 5. The displacements in the x- and y-directions as a function of time for two circular particles sedimenting in a two-dimensional channel at $Re = 5.6$.

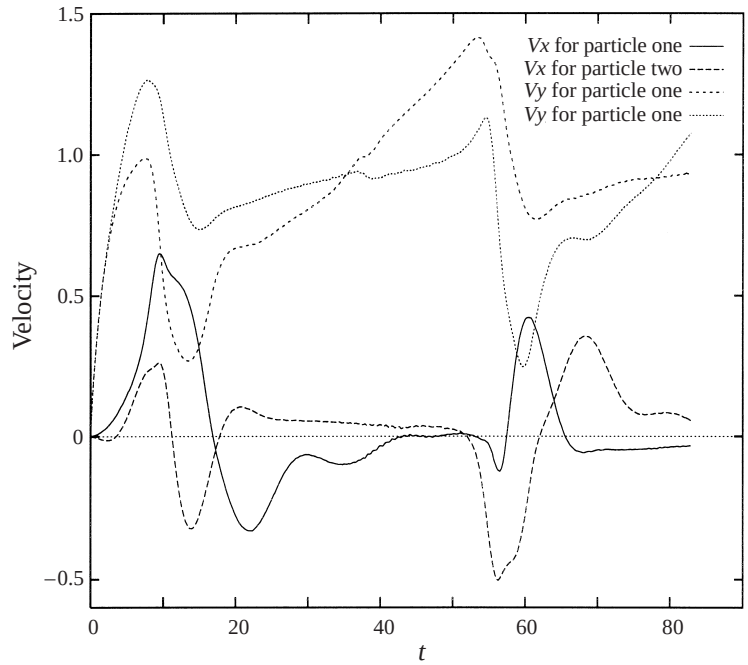

FIGURE 6. The velocities in the x- and y-directions as a function of time for two circular particles sedimenting in a two-dimensional channel at $Re = 5.6$.

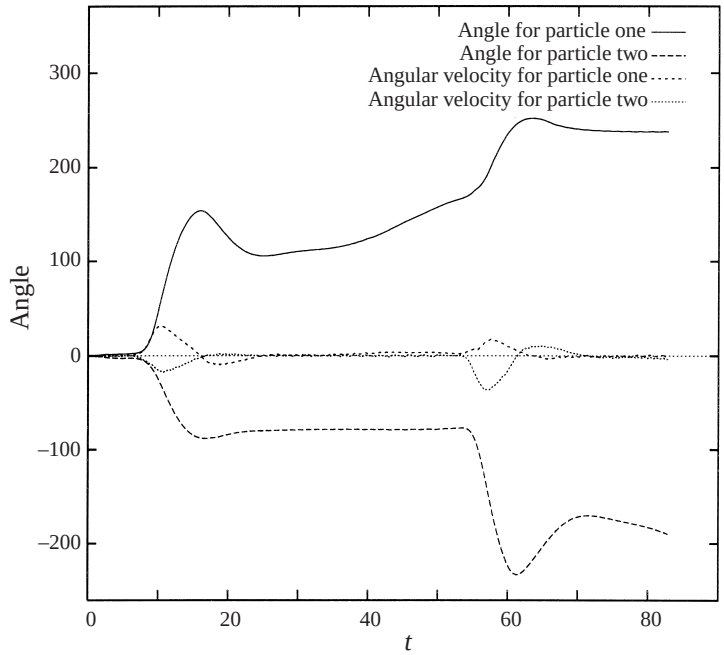

FIGURE 7. The rotation angles and angular velocities as a function of time for two circular particles sedimenting in a two-dimensional channel at $Re = 5.6$.

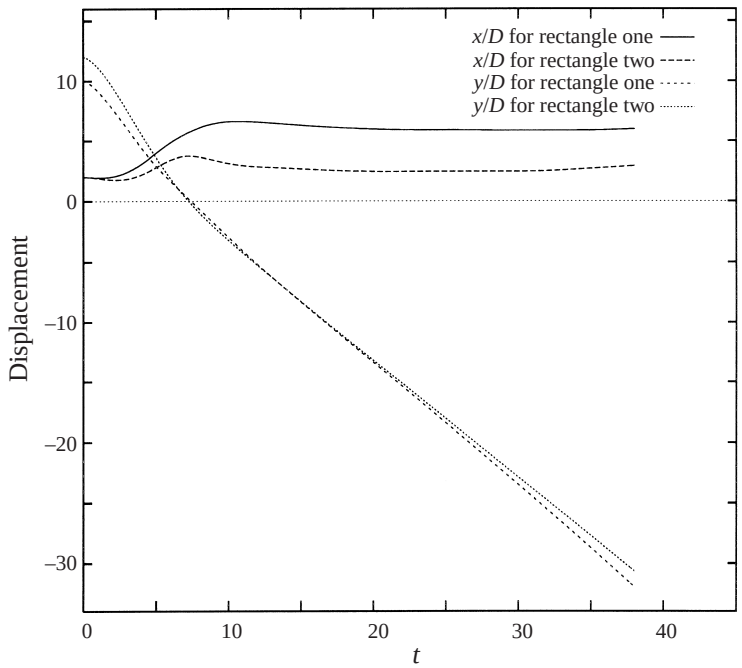

FIGURE 8. The displacements in the x- and y-directions as a function of time for two rectangular particles sedimenting in a two-dimensional channel at $Re = 1.1$.

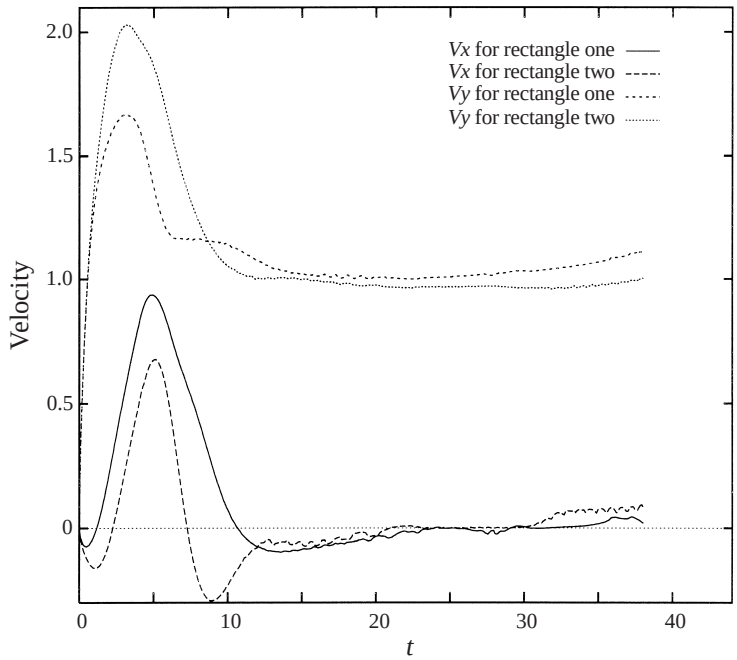

FIGURE 9. The velocities in the x- and y-directions as a function of time for two rectangular particles sedimenting in a two-dimensional channel at $Re = 1.1$.

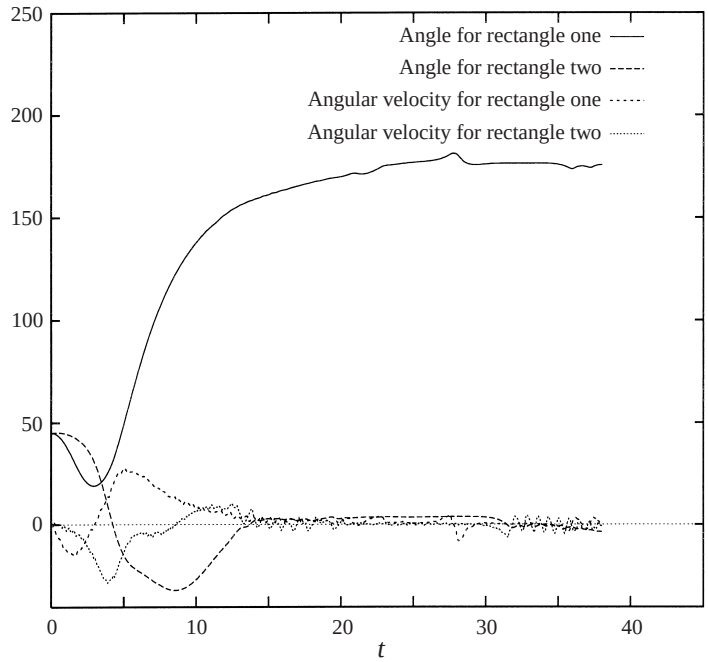

FIGURE 10. The rotation angles and angular velocities as a function of time for two rectangular particles sedimenting in a two-dimensional channel at $Re = 1.1$.

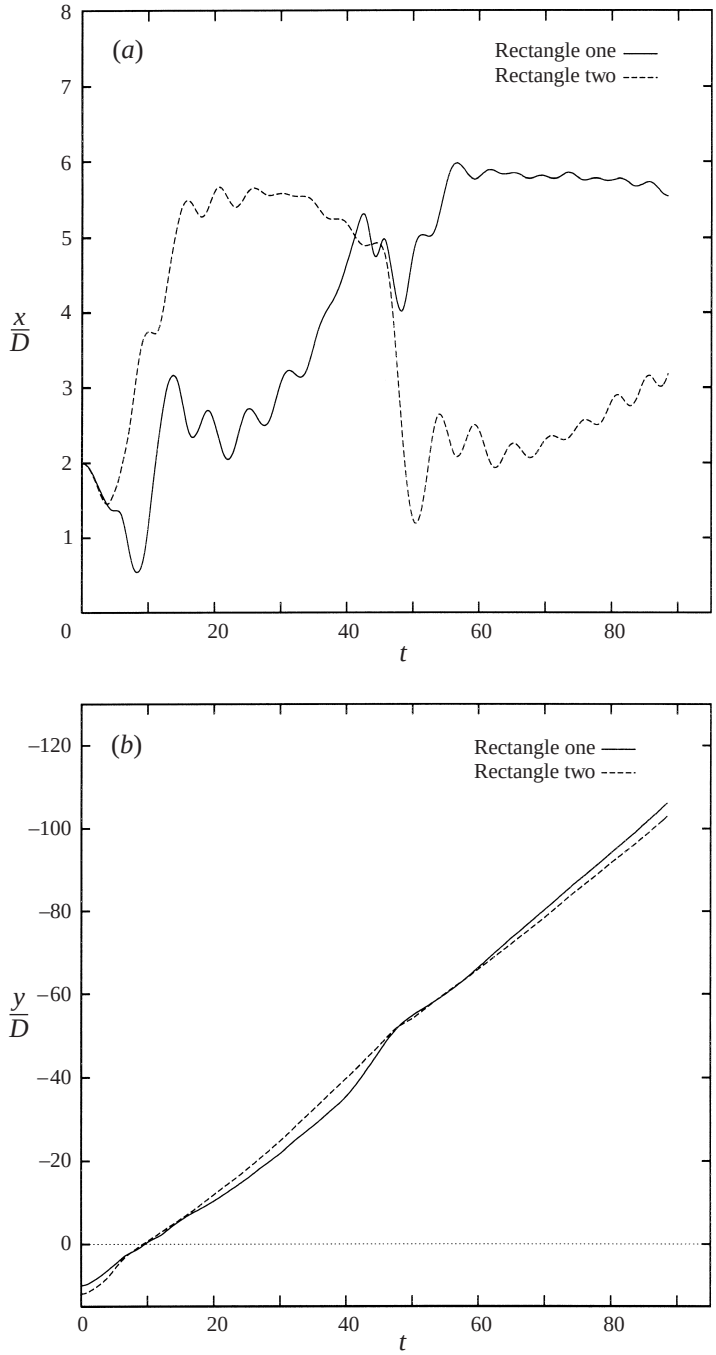

FIGURE 11. The displacements in the x- and y-directions as a function of time for two rectangular particles sedimenting in a two-dimensional channel at $Re = 31.7$.

in the settling direction twice. The velocity in the settling direction increases when the trailing particle catches up with the leading particle as shown in figure 6. The large variation of the velocities during kissing reflects the strong interaction when two particles approach each other. Meanwhile, they rotate in different directions.

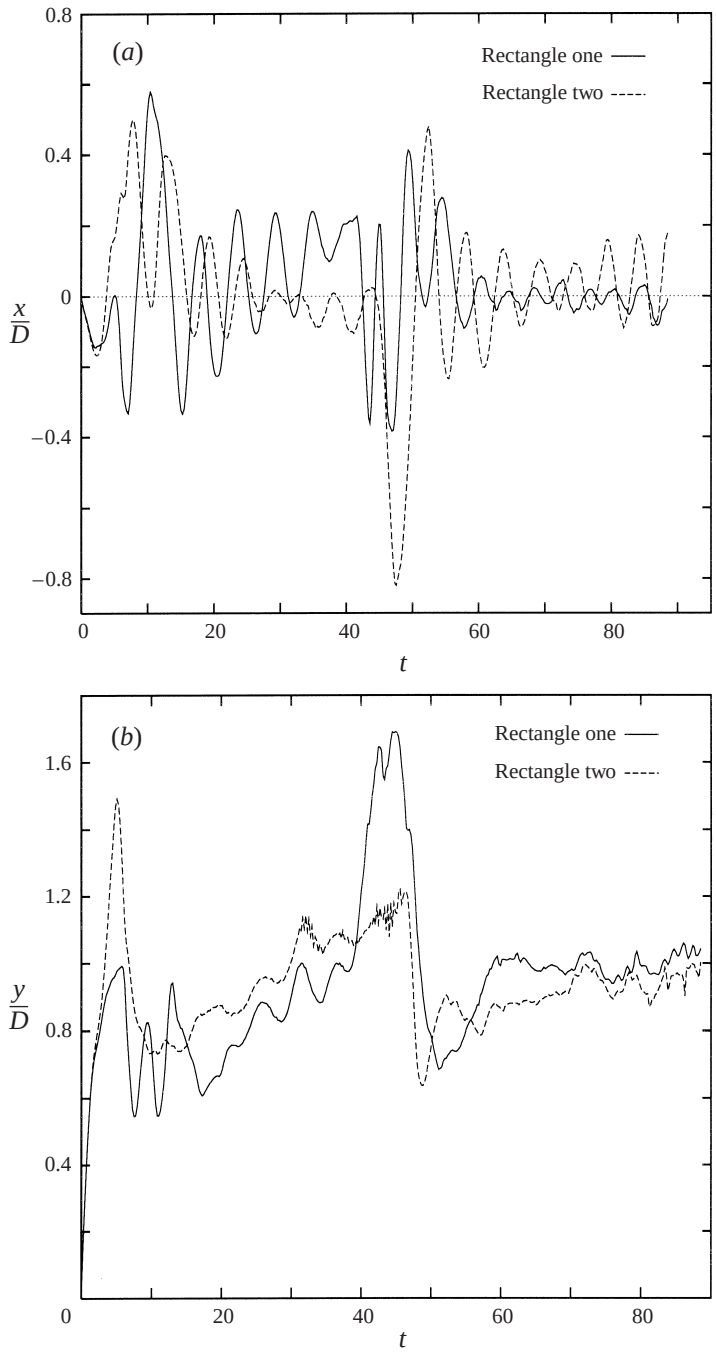

FIGURE 12. The velocities in the x- and y-directions as a function of time for two rectangular particles sedimenting in a two-dimensional channel at $Re = 31.7$.

The original leading particle rotates in the counter-clockwise direction, it seems to climb the channel wall as it settles, while the trailing particle rotates in the clockwise direction. They almost stop rotating after $t = 70$ as shown in figure 7. DKT is fully reproduced by this simulation.

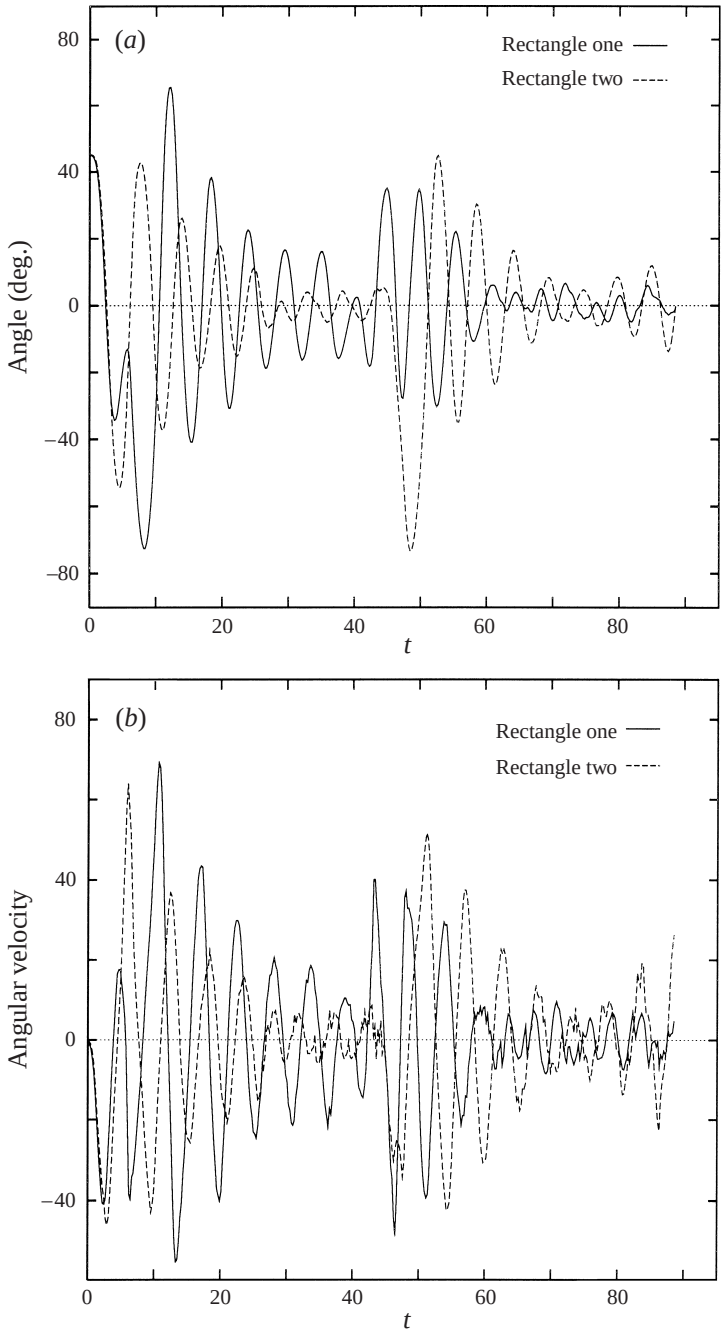

FIGURE 13. The angles and angular velocities as a function of time for two rectangular particles sedimenting in a two-dimensional channel at $Re = 31.7$.

3.3. *Sedimentation of two rectangular particles*

Before conducting a three-dimensional simulation, let us examine the behaviour of two rectangular particles sedimenting in a two-dimensional channel.

The size of the simulation box is 161×540 and the size of the rectangular particle

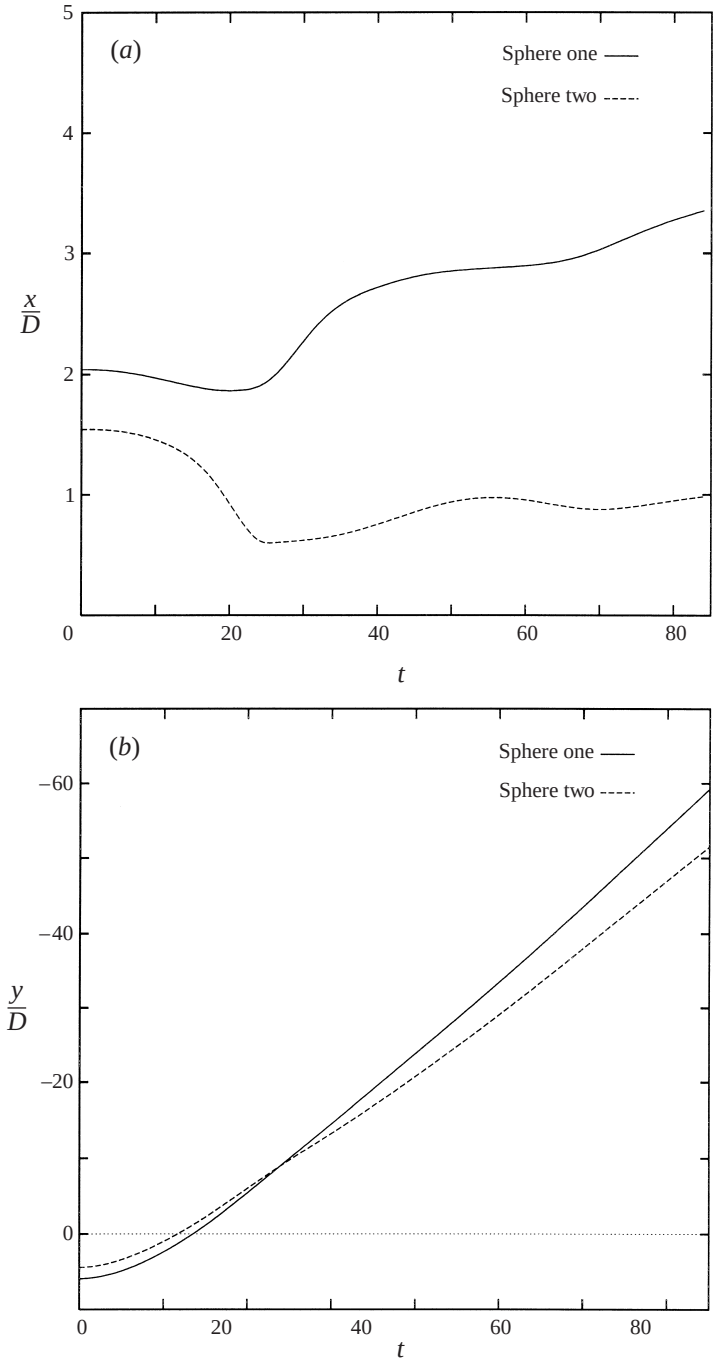

FIGURE 14. The displacement in (*a*) the *x*-direction and (*b*) the *y*-direction as a function of time with final $Re = 13.1$.

is 20×10. The outflow boundary is placed at $y = 540$ and the inflow boundary at $y = 0$ initially. The two rectangular particles are $2D$ apart along the gravity direction and aligned at $x = 0.25W$. The width W of the simulation box is 8 times of the length D of the longer edge of the particle. The outflow boundary is always kept at

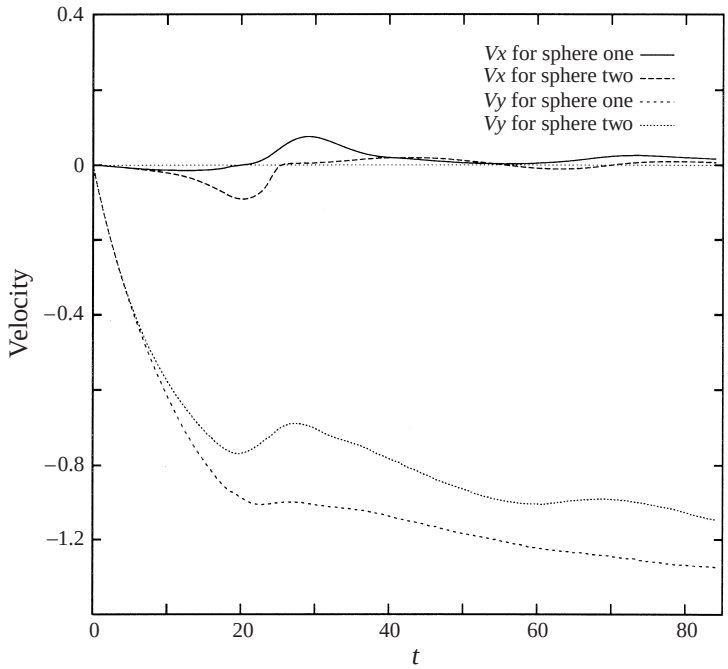

FIGURE 15. The velocities in the x- and y-directions as a function of time with final $Re = 13.1$.

$15D$ behind the trailing particle and the inflow boundary is always at $10D$ ahead of the leading particle during the simulation. The flow velocities at the boundaries are the same as before. The ratio of the solid density to the fluid density is 2 and the final particle Reynolds number for the simulation is $Re = 1.1$. The results are shown on figure 8 to figure 10. DKT occurs quickly at $t = 7$ and $t = 13$ for the rectangular particles as shown in figure 8.

It seems that a steady solution is obtained for this case. After one oscillation, the particles reach a steady state. The velocity in the x-direction approaches zero and the velocity in the y-direction becomes a constant. The original leading particle rotates in the counter-clockwise direction and approaches 180°. The other rectangular particle rotates in the opposite direction, then returns to zero. Both particles turn horizontal due to the turning couples on the long body as they settle steadily.

Another simulation is carried out at the same conditions except that the particle Reynolds number is $Re = 31.7$. A strong oscillation is obtained and is shown in figures 11 to 13. DKT occurs during sedimentation. There are four crossings at approximately $t = 8$, $t = 15$, $t = 49$ and $t = 56$ as shown in figure 11. The velocities in the x- and y-directions actively oscillate as shown in figure 12. The amplitude of the velocity oscillation becomes larger when they are kissing. The angles of the two particles oscillate around zero showing that the longer edges of the rectangular turn horizontal. The two particles rotate in opposite directions and have a larger oscillation amplitude when they are kissing. Then, the amplitude decreases after tumbling as shown in figure 13. When the next DKT occurs, the amplitude of velocity of particles including angular velocity increases again. Such a cycle is repeated.

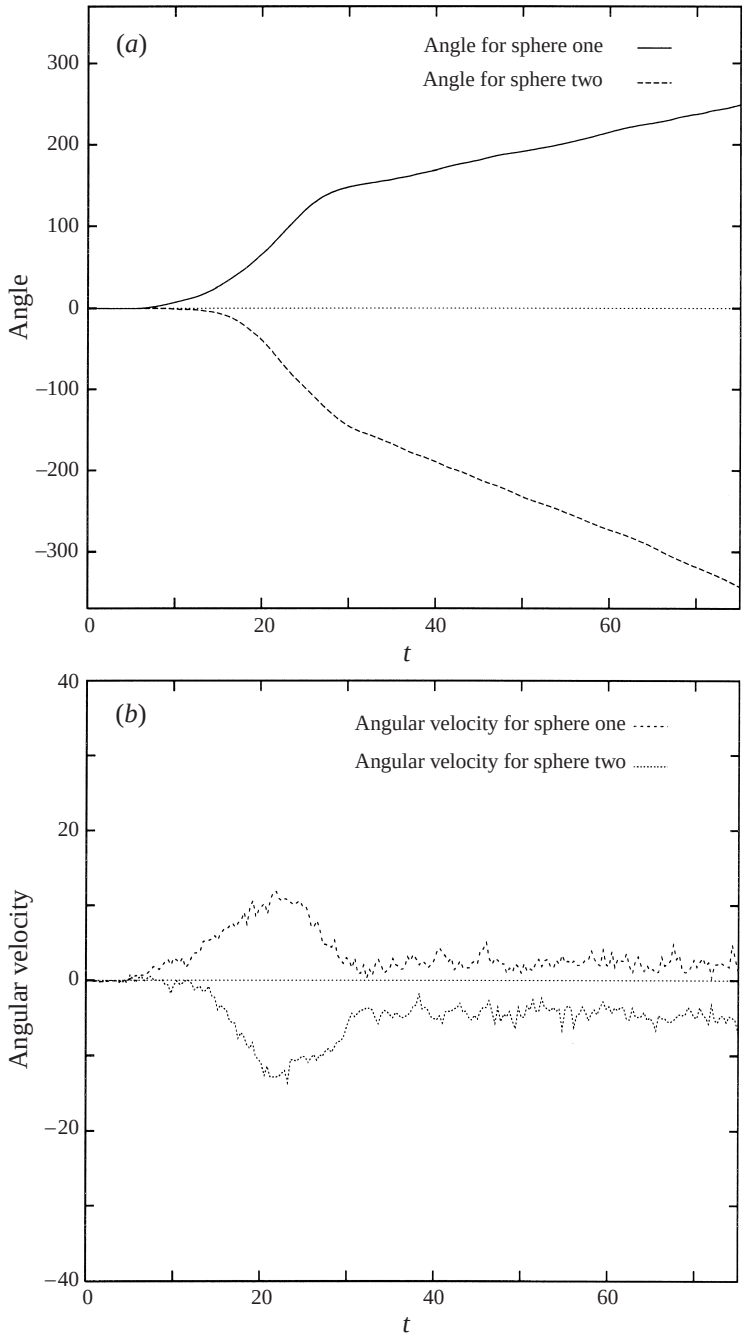

FIGURE 16. (*a*) The rotation angles and (*b*) angular velocities as a function of time with final $Re = 13.1$.

3.4. *Sedimentation of two spherical three-dimensional particles*

Sedimentation of two spherical particles under gravity, in a tube with square cross-section, is simulated. The size of the simulation box is $64 \times 80 \times 64$. The gravity force is along the y-axis in the negative direction. The diameter D of the spherical

particles is 12.4 and their initial coordinates in the x- and y-directions can be read from figure 14(a,b) and those in the z-direction are in the centre of channel, which never changed during sedimentation due to wall effects. The ratio of the density of the spherical solid particles, to the fluid density is 1.005. As the spheres fall in the tube, one of them is accelerated to a higher velocity than other sphere, due to a low pressure caused by the wake of the leading sphere. The trailing particle catches the leading particles at $t = 23$ as shown in figure 14(b). The velocities in the x- and y-directions as a function of time are shown in figure 15 and the angles and angular velocities as a function of time are shown in figure 16. The large change of velocities indicates the strong interaction when two spheres approach each other. The final particle Reynolds number is $Re = 13.1$ for this simulation. Again, drafting, kissing and tumbling are reproduced in this three-dimensional simulation correctly.

4. Conclusions

(a) The LB method has been developed to simulate particles in finite-Reynolds-number flows. The method is accurate, compared with the finite-element results. Using this method, the simulations are dynamically stable.

(b) The LB results obtained by using the improved approach for an ellipse sedimenting at $Re = 0.31$, 0.82 and 16.8 are compared with the results obtained with the finite-element method. The present results are in excellent agreement with the finite-element results. Therefore, the LB method is shown to be reliable for both zero- and finite-Reynolds-number flows.

(c) DKT is reproduced for two circular particles in a two-dimensional channel.

(d) DKT occurs for two rectangular particles. A steady solution is obtained at small particle Reynolds number and a dynamically oscillating solution is observed at high Reynolds numbers. The long edges turn horizontal for these rectangular particles.

(e) Sedimentation of two three-dimensional spherical particles has been simulated in a tube with square cross-section and DKT is correctly reproduced.

The author is most grateful to Professor A. J. C. Ladd for his many valuable suggestions, several readings of the manuscript. The author also greatly appreciates Professor Daniel Joseph for his critical reading of the manuscript and valuable discussions. I am deeply indebted to Dr Peter Huang and Professor Daniel Joseph who kindly solved the problem of sedimentation of an ellipse at $Re = 16.8$ by using their program and gave the results to me. Otherwise, the comparison would not be possible. This work is partially supported by an award (grant number CTS950038P) from the Pittsburgh Supercomputing Center.

REFERENCES

Aidun, C. K. & Lu, Y. 1995 Lattice Boltzmann simulation of solid suspensions with impermeable boundaries. *J. Statist. Phys.* **81**, 49.

Aidun, C. K., Lu, Y. & Ding, E. 1998 Direct analysis of particulate suspensions with inertia using the discrete Boltzmann equation. *J. Fluid Mech.* **373**, 287.

Aidun, C. K. & Qi, D. 1998 A new method for analysis of the fluid interaction with a deformable membrane. *J. Statist. Phys.* **90**, 145.

Allen, M. P. & Tildesley, D. J. 1987 *Computer Simulation of Liquids.* Clarendon.

Brady, J. F. & Bossis, G. 1988 Stokesian dynamics. *Ann Rev. Fluid Mech.* **20**, 111.

Chang, C. & Powell, R. L. 1993 Dynamic simulation of bimodal suspensions of hydro-dynamically interacting spherical particles. *J. Fluid Mech.* **253**, 1.

Chen, H., Chen, S. & Matthaeus, W. H. 1992 Recovery of the Navier–Stokes equations using a lattice gas Boltzmann method. *Phys. Rev.* A **45**, 5339.

Dahlburg, J. P., Montgomery, D. & Doolen, G. 1987 Noise and compressibility in lattice-gas fluids *Phys. Rev.* A **36**, 2471.

d'Humieres, D. & Lallemand, P. 1987 Numerical simulation of hydrodynamics with lattice gas automata in two dimension. *Complex Systems* **1**, 599.

d'Humieres, D., Lallemand, P. & Frisch, U. 1986 Lattice gas model for 3D hydrodynamics. *Europhys. Lett.* **2**, 291.

Evans, D. J. 1977 On the presentation of orientation space. *Mol. Phys.* **34**, 317.

Evans, D. J. & Murad, S. 1977 Singularity-free algorithm for molecular dynamics simulation of rigid polyatomics. *Mol. Phys.* **34**, 327.

Feng, J., Hu, H. H. & Joseph, D. D. 1994*a* Direct simulation of initial value problems for the motion of solid bodies in a Newtonian fluid. Part 1. Sedimentation. *J. Fluid Mech.* **261**, 95.

Feng, J., Hu, H. H. & Joseph, D. D. 1994*b* Direct simulation of initial value problems for the motion of solid bodies in a Newtonian fluid. Part 2. Couette and Poiseuille flows. *J. Fluid Mech.* **277**, 271.

Frisch, U., d'Humieres, D., Hasslacher, B., Lallemand, P., Pomeau, Y. & Rivet, J.-P. 1987 Lattice gas hydrodynamics in two and three dimensions. *Complex Systems.* **1**, 64.

Gear, C. W. 1971 *Numerical Initial Value Problems in Ordinary Differential Equations*. Prentice-Hall.

Goldstein, H. 1980 *Classical Mechanics*. Addison-Wesley.

Gunstensen, A. K. & Rothman, D. H. 1991*a* A lattice-gas model for immiscible fluids. *Physica* D **47**, 47.

Gunstensen, A. K. & Rothman, D. H. 1991*b* A galilean-invariant two-phase lattice gas. *Physica* D **47**, 53.

Hu, H. H. 1996 Direct simulation of flows of solid-liquid mixtures. *Intl J. Multiphase Flow* **22**, 335.

Hu, H. H., Joseph, D. D. & Crochet, M. J. 1992 Direct simulation of fluid particle motions. *Theoret. Comput. Fluid Dyn.* **3**, 285.

Huang, P. Y., Hu, H. H. & Joseph, D. D. 1998 Direct simulation of the sedimentation of elliptic particles in Oldroyd-B fluids. *J. Fluid Mech.* **362**, 297.

Hughes, T. J. R., Franca, L. P. & Mallet, M. 1987 A new finite element formulation for computational fluid dynamics: VI convergence analysis of the generalizes SUPG for simulation for linear time-dependent multi-dimensional advective–diffusive systems. *Comput. Mech. Appl. Mech. Engng* **69**, 277.

Johnson, A. A. & Tezduyar T. E. 1997 3D simulation of fluid-particle interactions with the number of particles reaching 100. *Comput. Meth. Appl. Mech. Engng.* **145**, 301.

Joseph, D. D., Fortes, A. F., Lundgreen, T. S. & Singh, P. 1987 Nonlinear mechanics of fluidization of beds of spheres cylinders and disks in water. In *Advances in Multiphase Flow and Related Problems* (ed G. Papanicolau), SIAM, p. 101.

Ladd, A. J. C. 1994*a* Numerical simulations of particulate suspensions via a discretized Boltzmann equation. Part 1. Theoretical foundation *J. Fluid Mech.* **271**, 285.

Ladd, A. J. C. 1994*b* Numerical simulations of particulate suspensions via a discretized Boltzmann equation. Part 2. Numerical results. *J. Fluid Mech.* **271**, 311.

Ladd, A. J. C. 1996 Hydrodynamic screening in sedimenting suspensions of non-Brownian spheres. *Phys. Rev. Lett.* **76**, 1392.

Ladd, A. J. C. 1997 Sedimentation of homogeneous suspensions of non-Brownian spheres. *Phys. Fluids* **9**, 491.

Ladd, A. J. C., Colvin, M. E. & Frenkel, D. 1988 Application of lattice-gas cellular automata to the Brownian motion of solids in suspension. *Phys. Rev. Lett.* **60**, 975.

Ladd, A. J. C. & Frenkel, D. 1990 Dissipative hydrodynamic interactions via lattice-gas cellular automata. *Phys. Fluids* A **2**, 1921.

McNamara, G. & Zanetti, G. 1988 Use of Boltzmann equation to simulate lattice-gas automata. *Phys. Rev. Lett.* **61**, 2332.

Qi, D. W. 1997*a* Non-spheric colloidal suspensions in three-dimensional space. *Intl J. Mod. Phys.* C **80**, 98.

Qi, D. W. 1997*b* Computer simulation of coating suspensions. In *Tappi Fundamental Coating Symposium* 201. Tappi.

Qi, D. W. 1997*c* Modeling of fluid transport in an anisotropic fiber network. *J. Tech. Assoc. Austral. NZ Pulp Paper Indust.* **50**, 319.

Qian, Y. 1990 PhD thesis, de l'Universite, Pierre et Marie Curie.

Qian, Y., d'Humieres, D. & Lallemand, P. 1992 Lattice BGK models for Navier–Stokes equation. *Europhys. Lett.* **17**, 479.

Tezduyar, T. E., Liou, J., Behr, M. & Mittal, S. 1992 A new strategy for finite element computations involving moving boundaries and interfaces- the DSD/ST procedure: I. The concept and the preliminary numerical tests. *Comput. Mech. Appl. Mech. Engng* **94**, 339.

Wolfram, S. 1986 Cellular automaton fluids 1: Basic theory. *J. Statist. Phys.* **45**, 471.